

Ab INITIO STUDY OF NEUTRAL OXYGEN VACANCIES IN RUTILE TiO₂

R. Plugaru^a, M. Artigas^b, N. Plugaru^{b,c}

^aNational Institute for R&D in Microtechnology-IMT Bucharest, PO-BOX 38-160, 023573 Bucharest, Romania
E-mail: rodica.plugin@imt.ro

^bDptmo. Ciencia y Tecnologia de Materiales y Fluidos, Centro Politecnico Superior (CPS),
Universidad de Zaragoza, c/ Maria de Luna 3, 50018 Zaragoza, Spain

^cNational Institute of Materials Physics, P.O.Box MG-07, Bucharest-Magurele 77125, Romania

Abstract—We present results of *ab initio* supercell calculations performed in the DFT-L(S)DA framework on rutile TiO₂ phase with neutral oxygen vacancies (OVs), in the low defect concentration range (≤ 6.25 at.%). The different OVs distributions in the supercell allow us to determine the localization and structure of the vacancy-induced states, the effect of vacancy concentration on the occupation numbers, as well as vacancy energetics. The present study benefits of the high accuracy in the total energy and band structure calculations of the full potential method utilized.

Keywords: *Ab initio* calculations, L(S)DA, rutile TiO₂, oxygen vacancies.

1. INTRODUCTION

Semiconductor oxides for advanced opto- and magneto-electronic devices are extensively investigated because their intrinsic properties can significantly be controlled by defects and impurity atoms. Among the materials of high interest is the titanium dioxide, TiO₂ [1-4], which shows electronic, magnetic and optical behavior strongly dependent on crystal structure and chemical composition, with emphasis on the oxygen stoichiometry [5, 6].

In search of means by which the oxygen deficiency may be used to tune the material optical properties [7], the present computational study is devoted to understand the effect of oxygen vacancies (OVs) on the electronic structure of rutile TiO₂, and bears a twofold motivation. Firstly, we aim to outline defect (OVs) imprints on the electronic band structure and find favourable OVs distributions. This may also be useful in the interpretation of spectroscopic data, whenever unambiguous identification of the transitions involving the defect states is rather difficult only by experiment.

However, the theoretical results on the localization of the OVs induced bands turn up to be affected by the intrinsic drawbacks inherent to the particular computational method used. Most of the calculations on bulk oxides are performed in the L(S)DA (Local (Spin) Density Approximation) which was shown to underevaluate the band gap due to self-interaction error and the fact that the potential is orbital-independent [8]. Recent theoretical progress has led to

refined SIC (Self Interaction Correction) and L(S)DA+U functional methods [9] in order to predict correct band gaps and absolute positions, in agreement with the experimental data. However, even if there is consensus on the physical reasons and appropriateness of these approaches, the results still are dependent on the technical details of the particular implementation. Therefore, our second goal has been to compare the results given by the *ab initio* code used in the present calculations with other L(S)DA results using the same parametrization of exchange and correlations.

The accuracy in the energy associated with the defect state may be increased by taking some precautions. Thus, we performed our study in the low concentration range, less than 6.25 at.% OVs, since higher defect concentration determines significant defect-defect interactions (which make necessary non-trivial corrections to the final results) and also stress in the crystal lattice, the relaxation of which is difficult to achieve in low symmetry supercells with tens of inequivalent lattice sites.

2. METHODOLOGY

We performed total energy and band structure calculations in the Local (Spin) Density Approximation (LSDA) using the Full Potential Local-Orbital (FPLO) band structure code [10]. FPLO is an all-electron scheme based on the method of linear combination of nonorthogonal overlapping local orbitals and uses a minimum valence basis set. It provides high accuracy in total energy calculations, being computationally efficient, at the same time, which is particularly useful for supercell calculations. We used the basis sets: for Ti, semicore (3s3p) and valence 4s4p3d states, and for O, semicore 1s, valence 2s2p and polarization 3d states, to achieve the basis completeness. The neutral oxygen vacancies were introduced as empty spheres with 1s2p3d polarization states. The exchange-correlation potential was treated in the parametrization of Perdew and Wang [11]. The site-centered potentials and densities were expanded in spherical harmonics up to $l_{\max}=12$. The check of the total energy convergence with respect to the k-mesh integrations for each supercell showed that a Brillouin zone sampling of $8\times 8\times 8=512$ k-points ensures a satisfactory level of convergence (at least 0.001 eV);

consequently, we used this parameter in the calculations reported below.

The rutile TiO_2 structure has the tetragonal symmetry of space group P 42/mnm (S.G. 136). The structure consists of infinite chains of edge-linked TiO_6 octahedra which share single corners, see Fig.1.

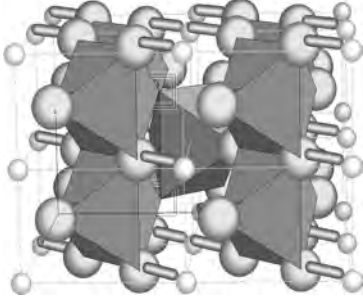


Fig. 1. Rutile TiO_2 structure. Larger light circles stand for oxygen and smaller dark ones for titanium. The octahedral coordination of Ti ions and the apical Ti-O bonds are shown. The image corresponds to the $2 \times 2 \times 2$ supercell labelled as C2 in the text.

The Ti-O apical bonds are longer than the four equal Ti-O bonds in the equatorial plane of the distorted octahedron. Oxygen atoms have in-plane coordination of 3 Ti atoms.

We performed the geometry optimization of the basic cell, including two lattice constants and one internal coordinate, starting from the experimental parameters given in [12]. The equilibrium volume was obtained for a and c lattice constants smaller by 0.53% than the experimental ones and the oxygen coordinate $u = 0.304$. A fit of the total energy versus volume, $E(V)$, plotted in Fig. 2, to the Murnaghan equation [13]:

$$E(V) = \frac{B_0 V}{B_0 (B_0 - 1)} \left[B_0 \left(1 - \frac{V_0}{V} \right) + \left(\frac{V_0}{V} \right)^{B_0} - 1 \right] + E_0$$

gives the values 247 GPa and 4.38 for the bulk modulus and its pressure derivative, in fair agreement with the experimental and calculated data (see ref.[14] and the references cited therein).

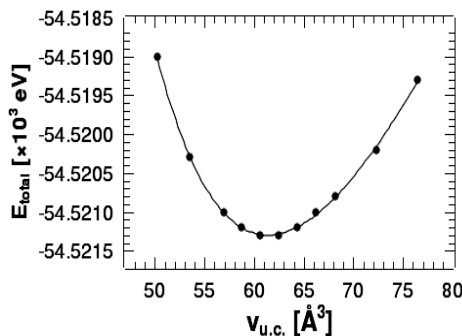


Fig. 2. Calculated $E(V)$ values with a fit using the Murnaghan equation.

Supercells $2 \times 2 \times 2$ of the basic cell at the equilibrium volume, see Fig.1, with several OV distributions were used as structural models in the calculations: *i*) supercell A, containing a single vacancy, illustrates the layout of 3.12% isolated OVs.; *ii*) supercell B, with 6.25 % OVs, with large separation distance (more than one lattice constant) between the OVs to probe the onset of vacancy-vacancy interactions and finite size effects, and *iii*) supercells C1 and C2, also with 6.25 % OVs arranged as isolated pairs with perpendicular and parallel orientation, respectively, to the crystallographic c -axis, to investigate symmetry and clustering effects. In all the cases we relaxed the atomic positions of the nearest neighbors (nn) to the OV sites.

3. DISCUSSION

A comparison between the total energy values in LDA and LSDA calculations for the oxygen defective cells indicated that the ground state is non magnetic for OVs concentration range up to 6.25 %. The LSDA treatment also predicted half metallic behavior in pure rutile, which is a computational artifact, similarly to that obtained for pure ZnO [15]. Consequently, in what follows we refer only to the results of the LDA treatment.

The total and element projected density of states (DOS) for the stoichiometric rutile are plotted in Fig.3.a. Our calculations predict a direct band gap of 1.71 eV, value close to other LDA results [5,14,16] but significantly undervalued with respect to the experimental value, 3.05 eV. The lower valence bands at about -17 eV are predominantly of O 2s character, see Fig.3.b. The upper valence bands are formed by mainly O 2p orbitals hybridized with Ti 3d orbitals, yielding a band width of 6.07 eV. The conduction bands below 8 eV consist mainly of Ti 3d states, hybridized with O 2p states, see Fig.3.c. and show two distinct structures, below and above 4.5 eV. The conduction bands above 8 eV have mainly s and p character. In the stoichiometric rutile the conduction bands are empty. These features fairly agree with results of previous calculations, e.g. [16-18].

It was derived from experiment that the OV in TiO_2 serves as a doubly ionizable donor, contributing with two electrons to the conduction band. This is supported by the results of present calculations. The density of states for supercell A are plotted in Figs.4.a-c. The Fermi level is shifted to the bottom of the conduction band and the defect induced states, with s character and a population of 0.395 electrons, are observed at -0.100 eV. We find a density of states at the Fermi level $N(E_F) = 0.7336$ states/eV/cell. The main contributions to the defect bands arise from Ti 3d orbitals, from the only two Ti sites each with a single vacancy nearest neighbor.

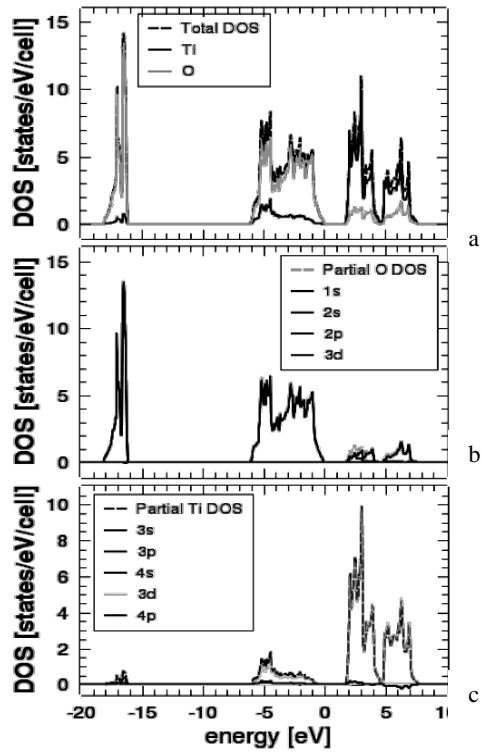


Fig. 3. Total and element-projected DOS, a), Partial and angular momentum-projected O DOS, b) and Partial and angular momentum-projected Ti DOS, c) of stoichiometric rutile TiO_2 . The Fermi level is at 0 energy.

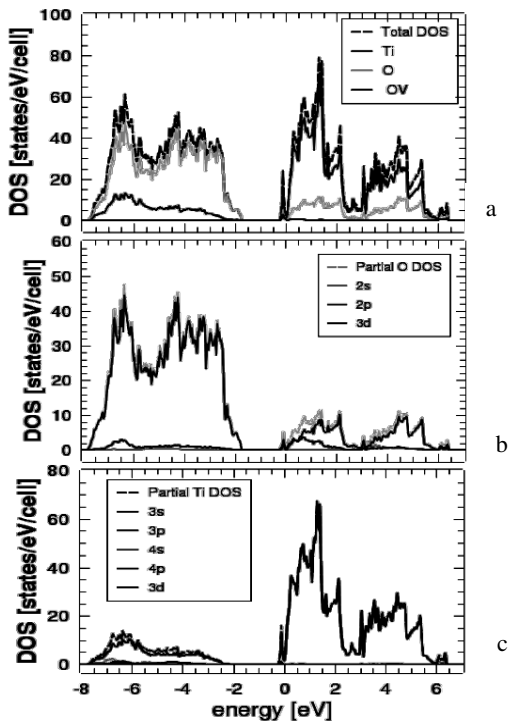


Fig. 4. Total and element-projected DOS, a), Partial and angular momentum-projected O DOS, b), and Partial and angular momentum-projected Ti DOS, c) for 3.1 % OVs, supercell A. The Fermi level is at 0 energy.

The density of states for supercell B, plotted in Fig.5.a, reveal similar features as observed for supercell A, but show a comparatively broadened defect band centred at -0.220 eV. In this case (still isolated vacancies but double concentration with respect to A), one may expect that the defect band broadening is due to defect-defect spurious electrostatic interactions as well as finite cell size effects. The density of states at the Fermi level $N(E_F)=6.084$ states/eV/cell, the excess charge at the OV site is 0.379 electrons and the defect states have s orbital symmetry.

Supercells C1 and C2 are illustrative for the clustering of defects, as the defect-defect distance is smaller than the length of the basic cell. However, the DOS plots in Figs.5.b and 5.c show different structures of the defect induced states. In the case of supercell C2 (see Fig.5.c) the defect level is situated at -0.140 eV and the DOS bears the general characteristics observed in supercells A and B. We find that $N(E_F)=2.7516$ states/eV/cell and the excess charge of 0.355 electrons at the defect site.

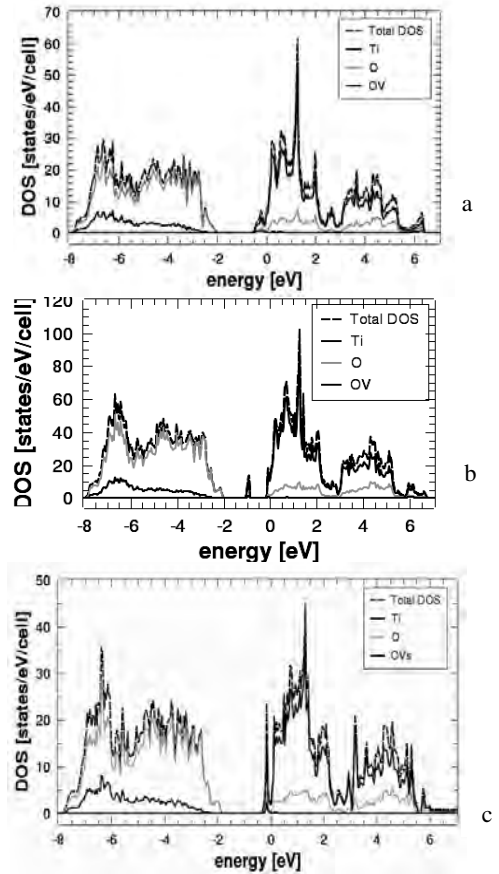


Fig. 5. Total and element-projected DOS for 6.2 % OVs distributed as: isolated vacancies, supercell B, a), OV pairs in supercell C1, b), and supercell C2, c) (see text for details). The Fermi level is at 0 energy.

In the case of supercell C1, the particular OV pair layout determines two different environments at Ti

sites. Thus, the Ti ions with a single vacancy nearest neighbor have a major contribution (Ti 3d states) at the shallow defect level at -0.100 eV. In the primitive cell there is also a Ti site with two OV nn at the apices of the octahedron around this ion, which has the main contribution at the deeper defect level, situated at -0.940 eV in the gap. The density of states at the Fermi level is $N(E_F)=13.609$ states/eV/cell. Both defect levels have s orbital symmetry and equal populations, of 0.254 electrons.

One has to apply several corrections to the total energy values before attempts to compare these data are made [9]. At the same time, the resulting lattices belong to different crystal classes, the k- mesh has a different topology in each case and that matters for comparing results. Bearing this in mind, we derive some preliminary information from a comparison of the total energy values given by the code: *i*) the total energy calculated for supercell C2 is lower by 2.031 eV than the value for C1, which suggests that the layout with OV pairs oriented along [001] direction is more stable than that with the vacancy pair orientation along [110]; *ii*) a comparison between the total energy values for the B and C2 supercells reveals a difference of only -0.133 eV, which eventually indicates that the isolated OV scenario (B) is more stable than the clustering one (C2), at 6.25 % OVs in the system.

4. CONCLUSIONS

We performed ab initio calculations using the FPLO code to explore the effect of neutral oxygen vacancies on the rutile TiO₂ electronic structure. No magnetic solution was found for OVs in bulk rutile with a concentration ≤ 6.25 at. %. In the structures labelled A, B and C2 herein, in which Ti ions have only one vacancy site nearest neighbor, the defect band appears centred at energies between -0.100 and -0.220 eV, just below the bottom of the conduction band. The Fermi level is "pinned" between the defect band and the CB bottom. For the OVs arrangement in supercell C1 we found a second defect band located deeper in the gap at about -1.0 eV, corresponding to Ti sites with two OVs nn. In all cases the main contribution to the vacancy induced states arises from Ti 3d orbitals and the vacancy states have s character. We should mention that for the two vacancy concentrations investigated in this study the gap becomes a gap within the VB and is no longer the semiconductor gap in the proper sense of the word. Its width is slightly dependent on vacancy concentration.

To our knowledge this is the first study using the FPLO code of oxygen vacancies in a wide band gap semiconductor.

Acknowledgments—This work was supported by Project 11-048/18.09.2007 NANOXI Program financed by National Authority for Scientific Research. RP and NP gratefully acknowledge the support related to FPLO code from Dr. M. Richter and Dr. K. Koepernick, IFW Dresden e.V., Germany.

References

- [1] G. Mallia, N.M. Harrison, "Magnetic moment and coupling mechanism of iron-doped rutile TiO₂ from first principles", *Phys. Rev.*, **B75**, 2007, pp. 165201-11.
- [2] M. Subramanian, S. Vijayalakshmi, S. Venkataraj, R. Jayavel, "Effect of cobalt doping on the structural and optical properties of TiO₂ films prepared by sol-gel", *Thin Solid films*, **516**, 2008, pp. 3705-4366.
- [3] R. Plugaru, A. Cremades, J. Piqueras, "The effect of annealing in different atmospheres on the luminescence of polycrystalline TiO₂", *J. Phys. Condens. Matter*, **16**, 2004, pp. S261-S268.
- [4] R. Plugaru, Optical properties of nanocrystalline titanium oxide, *Thin Solid Films*, 11 April 2008, in press, 2008.
- [5] F.M. Hossain, G.E. Murch, L. Sheppard, J. Nowotny, "Ab initio electronic structure calculation of oxygen vacancies in rutile titanium dioxide", *Solid State Ionics*, **178**, 2007, pp. 319-325.
- [6] K. Onda, B. Li, H. Petek, "Two-photon photoemission spectroscopy of TiO₂ (110) surfaces modified by defects and O₂ or H₂O adsorbates", *Phys. Rev.*, **70**, 2004, pp. 045415-11.
- [7] E. Cho, S. Han, H.-S. Ahn, K.-R. Lee, S.K. Kim, C.S. Hwang, "First-principles study of point defects in rutile TiO_{2-x}", *Phys. Rev.*, **73**, 2006, pp. 193202-6.
- [8] R.M. Dreizler, E.K.U. Gross, "Density Functional Theory, An Approach to the Quantum Many-Body Problem", Springer-Verlag, Berlin, 1990.
- [9] R.M. Nieminen, "Supercell Methods for Defect Calculations, in Theory of Defects in Semiconductors", Springer-Verlag Berlin Heidelberg, 2007, p. 29.
- [10] K. Koepernick, H. Eschrig, "Full-potential nonorthogonal local-orbital minimum-basis band structure scheme", *Phys. Rev.*, **B 59**, 1999, pp. 1743-1757.
- [11] J.P. Perdew, Y. Wang, "Accurate and simple analytic representation of the electron-gas correlation energy", *Phys. Rev.*, **B 45**, 1992, pp. 13244-13249.
- [12] S.C. Abrahams, J.L. Bernstein, "Rutile: Normal Probability Plot Analysis and Accurate Measurement of Crystal Structure", *The Journal of Chemical Physics*, **55**, 1971, pp. 3206-3211.
- [13] V. Tyuterev, N. Vast, "Murnaghan's equation of state for the electronic ground state energy", *Comp. Mat. Sci.*, **38**, 2006, pp. 350-353.
- [14] J. Muscat, V. Swamy, N.M. Harrison, "First-principles calculations of the phase stability of TiO₂", *Phys. Rev.*, **B65**, 2002, pp. 224112-15.
- [15] T. Chanier, M. Sargolzaei, I. Opahle, R. Hayn, K. Koepernick, "LSDA+U versus LSDA: Towards a better description of the magnetic nearest-neighbor exchange coupling in Co- and Mn-doped ZnO", *Phys. Rev.*, **B73**, 2006, pp. 134418-7.
- [16] G.U. von Oertzen, A.R. Gerson, "The effects of O deficiency on the electronic structure of rutile TiO₂", *J. Phys. Chem. Solids*, **68**, 2007, pp. 324-330.
- [17] S.D. Mo, W.Y. Ching, "Electronic and optical properties of three phases of titanium dioxide: Rutile, anatase, and brookite", *Phys. Rev.*, **B51**, 1995, pp. 13023-13032.
- [18] B. Jiang, J. M. Zuo, N. Jiang, M. O'Keeffe, J.C.H. Spence, "Charge Density and Chemical Bonding in Rutile, TiO₂", *Acta Cryst.*, **A59**, 2003, pp. 341-350.